

A Fully Three-Dimensional Kinetic Particle-In-Cell Framework for Modeling Laser-Dielectric Interactions: Few-Cycle Pulse Damage

Joseph R. Smith¹, Ziyao Su², Simin Zhang², Charles Varin³, Vitaly E. Gruzdev⁴, and Enam A. Chowdhury²

¹Department of Physics, Marietta College, Marietta, Ohio 45750, USA

²Department of Materials Science and Engineering, The Ohio State University, Columbus, Ohio 43210, USA

³Cégep de l'Outaouais - CyberQuébec, Gatineau, QC, J8Y 6M4, Canada

⁴Department of Physics and Astronomy, University of New Mexico, Albuquerque, NM, 87106, USA

Abstract

We present a fully three-dimensional kinetic framework for modeling intense short pulse lasers interacting with dielectric materials. Our work modifies the open-source Particle-In-Cell (PIC) code EPOCH to include new models for photoionization and dielectric optical response. We use this framework to model the laser-induced damage of dielectric materials by few-cycle laser pulses. The framework is benchmarked against experimental results for bulk silica targets and then applied to model multi-layer dielectric mirrors with a sequence of simulations with varying laser fluence. This allows us to better understand the laser damage process by providing new insight into energy absorption, excited particle dynamics, and nonthermal excited particle distributions. We compare common damage threshold metrics based on the energy density and excited electron density.

1. Introduction

The 2023 Nobel Prize in Physics awarded to Pierre Agostini, Ferenc Krausz and Anne L'Huillier “for experimental methods that generate attosecond pulses of light for the study of electron dynamics in matter”^[1] and the 2018 National Academies of Science report^[2] that spurred the “Brightest Light Initiative”^[3] highlight the impactful science enabled by producing the shortest possible pulses of light^[4–6]. Recent advances in high-energy few-cycle pulse generation techniques^[7,8] allow us to probe new physical effects including those from carrier-envelope phase^[9–11] and to generate high laser intensities with moderate laser energies for applications such as relativistic plasma-based attosecond pulse generation^[12]. These developments motivate the design of optical components with higher Laser-Induced Damage Thresholds (LIDTs) for few to single-cycle pulses. The scaling of LIDT with laser fluence is generally well understood for the tens of picosecond to nanosecond regimes^[13], but is more complex for shorter pulses^[14], especially few-cycle pulses^[15,16].

Previous experimental work has explored the damage and ablation of SiO₂ using few-cycle ~800 nm wavelength pulses with durations of 5 fs^[15,17,18] and 7 fs^[16,19–21]. Re-

cently Kafka et al.^[18] determined the damage threshold for different optical components with a 5 fs pulse and Talisa et al.^[22] explored the damage and ablation of SiO₂/HfO₂ multilayer coatings with 8 fs pulses. As highlighted in the review by Nagy et al.^[8], post-compression techniques allow researchers around the world (e.g., Refs.^[12,23–25]) to generate few-cycle pulses, but traditional optics are easily damaged by these compressed pulses.

Understanding few-cycle pulse material interactions requires advances in computational and theoretical models. There has been significant work using one-dimensional Finite-Difference-Time-Domain (FDTD) simulations to model these interactions^[26], with recent efforts in two dimensions^[27,28]. FDTD simulations provide insight into the laser material interactions and can predict LIDT, but do not capture the nonthermal nature of excited electrons, nor do they capture their ballistic motion. To expand our understanding of the interaction dynamics, we use Particle-In-Cell (PIC) simulations^[29,30]. As with FDTD simulations, PIC codes solve Maxwell's equations on a computational grid. Additionally, PIC simulations statistically represent the neutral and excited particles in the simulation with a finite number of ‘macroparticles’^[29–31]. The charged particles are then advanced using the Lorentz force and additional physical effects including ionization and collisions are often added.

Correspondence to: Email: JosephRSmith@protonmail.com, Email: chowdhury.24@osu.edu

PIC simulations are commonly used to study laser-plasma interactions (e.g., Ziegler et al.^[321]) and increasingly being modified to simulate laser damage and related regimes. For example, Mitchell et al.^[33] model crater formation in metals due to femtosecond laser ablation, Cochran et al.^[34] model liquid-crystal plasma mirrors^[35], Déziel et al.^[36] study laser-induced periodic surface structures, and Ding et al.^[37] and Do et al.^[38] model plasmons using PIC. Interactions of lasers with nano/micro-scale structures in silicon and SiO₂ have been modeled with versions of the framework introduced in this work^[39,40] and recently Charpin et al.^[41] developed a similar framework to explore ionization in dielectrics. Our work builds on these efforts specifically for laser damage for few-cycle pulses by including the corrected Keldysh ionization model^[28,42,43], to account for ionization across a range of fluences. We are able to explore the nonthermal distribution of excited particles in the laser-damage regime using PIC, which improves our fundamental understanding of damage mechanisms.

In this work, we begin in Sec. 2 by introducing the modifications and extensions we have made to a PIC code to model laser-dielectric interactions. Then in Sec. 3 we discuss the material properties and simulation setup for both bulk and multi-layer targets. Next, in Sec. 4 we compare the predictions of this framework to existing experimental results and discuss expected damage threshold metrics. Then we apply the framework to the modeling of multi-layer mirrors in Sec. 5 and conclude in Sec. 6.

2. Particle-In-Cell Simulation Modifications

Our work extends the three-dimensional (3D) implementation of version 4.17.10 of the EPOCH^[31] PIC code, which is designed for the study of high energy density physics. EPOCH is a popular open-source PIC code that can scale to run on thousands of CPU cores, although we note that there are a variety of other open-source and proprietary PIC codes available with different features and implementations^[44] such as GPU operation (e.g., PIConGPU^[45] and WarpX^[46]). PIC simulations of laser-matter interactions are typically used to study only tens-to-hundreds of femtosecond timescales due to numerical instability issues and computational cost. As such, we focus on the initial laser-matter interaction and the resulting excited electron dynamics. For long-term dynamics and equilibration, one could use a final simulation state from PIC as the initial conditions for another model. For example, one could use the electron and ion temperatures in a two temperature model, or consider tabulated equation of state values^[16].

EPOCH includes multiple physics modules, but was not designed with laser-dielectric interactions in mind. Towards this goal, we have added a new photoionization model relevant for dielectric materials and a model for optical material properties as discussed in the next subsections.

2.1. Keldysh Photoionization

Our work extends the existing ionization framework already available in EPOCH^[31] to include the photoionization model developed by L. V. Keldysh^[42]. The Keldysh ionization model allows us to calculate probabilities for electron transitions from the valence to the conduction band in solids due to the electric field of a laser pulse^[47].

For a laser pulse with electric field amplitude E and frequency ω interacting with a material having band gap Δ and reduced electron-hole mass m^* , the Keldysh parameter is $\gamma = \omega \sqrt{m^* \Delta} / eE$, where $\gamma \gg 1$ is the multiphoton ionization regime and $\gamma \ll 1$ is in the tunneling regime^[42]. The Keldysh formulation is especially useful as it spans both regimes, which are often present when considering a laser induced damage experiment. For example, the peak electric fields in our simulations give values of γ ranging from about 0.3 to 0.9, which means the photoionization regime is neither multiphoton nor tunneling, suggesting that the full Keldysh formula should be utilized.

The Keldysh model is used in our simulations to calculate the probability that a given neutral macroparticle will ionize. When ionization occurs, a new electron macroparticle and corresponding ion macroparticle are created in place of the original macroparticle. Now we introduce the ionization rate equation used in our work. For brevity in the following expressions, we follow Refs.^[48,49] by introducing the variables $\gamma_1 = \gamma^2 / (1 + \gamma^2)$ and $\gamma_2 = 1 / (1 + \gamma^2)$. The effective band gap is then given by

$$x = \frac{2}{\pi} \frac{\Delta}{\hbar \omega} \frac{\epsilon(\gamma_2)}{\sqrt{\gamma_1}}. \quad (1)$$

We may then write the ionization rate W as

$$W[m^{-3}s^{-1}] = 2 \frac{2\omega}{9\pi} \left(\frac{m^* \omega}{\hbar \sqrt{\gamma_1}} \right)^{3/2} \times Q(\gamma, x) \exp\left(-\pi [x + 1] \frac{\kappa(\gamma_1) - \epsilon(\gamma_1)}{\epsilon(\gamma_2)}\right), \quad (2)$$

where κ and ϵ are complete elliptic integrals of the first and second kind, Φ is the Dawson integral, and

$$Q(\gamma, x) = \sqrt{\frac{\pi}{2\kappa(\gamma_2)}} \sum_{n=0}^{\infty} \exp\left(-n\pi \frac{\kappa(\gamma_1) - \epsilon(\gamma_1)}{\epsilon(\gamma_2)}\right) \times \Phi\left(\sqrt{\frac{\pi^2([\![x + 1\!] - x + n)}{2\kappa(\gamma_2)\epsilon(\gamma_2)}}}\right). \quad (3)$$

We note that this is the corrected version of the formulation, where the original contains a misprint as noted by Gruzdev^[43]. Using the uncorrected version can result in significantly different calculations^[28,43].

For our simulation framework, the Keldysh ionization

rate is evaluated in-situ¹ rather than interpolated from a tabulated form which facilitates accuracy over a wide range of fluences. We use the first 500 terms in this infinite sum in Eq. 3, which is sufficient for the regimes of interest in this paper, as illustrated in Appendix A, while limiting the computational cost. An adaptive approach to a prescribed tolerance could be employed in the future. Currently each macroparticle can only be ionized once.

While the Keldysh parameter depends on the laser amplitude E , the amplitudes of our pulses vary within the laser envelope. Moreover, each computational cell in a PIC simulation only considers the instantaneous electric field. To address this, we store the electric field magnitude at each time step using an array large enough to store an entire laser cycle on a rolling window, as suggested by Zhang et al.^[28]. Then the maximum field for the previous cycle is used to approximate the amplitude to calculate the ionization rate. This approach would encounter challenges for single-cycle pulses. In the future a more complex envelope model could be explored^[50].

2.2. Collisional Effects

We use the Pérez/Nanbu^[51,52] binary collision module already included in the EPOCH code to account for collisions. The collision frequency in EPOCH is calculated for a charged particle α with charge q_α scattering off a charged particle β as

$$\nu_{\alpha\beta} = \frac{(q_\alpha q_\beta)^2 n_\beta \ln(\Lambda)}{4\pi(\varepsilon_0 \mu)^2} \frac{1}{v_r^3}, \quad (4)$$

where n_β is the density (for particles of species β), $\ln(\Lambda)$ is the Coulomb Logarithm, $\mu = m_\alpha m_\beta / (m_\alpha + m_\beta)$ is the reduced mass, and v_r is a relative velocity^[31]. EPOCH extends the model to low temperatures following an approach by Pérez et al.^[51], Lee and More^[53]. More details can be found in Arber et al.^[31] and in the source files and documentation provided with the open-source EPOCH code². Collisions are included between all charged particles in the simulation. The Coulomb logarithm is calculated automatically with a fixed lower bound of 1.

EPOCH includes a collisional ionization routine designed for atoms^[31,54], but this is not well suited for impact ionization in dielectrics. A more appropriate ionization rate for our regime can be calculated with the approach by Keldysh^[55], although some of the input parameters to the models are not well reported and may require fitting of output results to experimental data^[41,56]. Impact ionization is reduced for shorter few-cycle pulses. Models by Petrov and Davis^[57] suggest collisional ionization dominates photoionization for fluences exceeding 0.4 J cm^{-2} , whereas

the Multiple-Rate-Equation (MRE) model by Rethfeld^[58] predicts this threshold to be 10 J cm^{-2} ^[49]. For this work, we do not include impact ionization, since we model few cycle pulses that are only 7 fs (fewer than 3 laser cycles) Full Width at Half Maximum (FWHM) in duration. We find good agreement with previous experiments without the need for impact ionization, but expect this to be an important consideration for longer pulses in future work.

2.3. Refraction

The optical properties of dielectrics are modeled using a spatially varying permittivity ε throughout the simulation box. At the beginning of the simulation the optical properties are stored in a matrix with the same size as the simulation grid. We then modified the field solver to include a spatially-dependent permittivity when advancing Maxwell's equations, following a similar approach to the one in the WarpX code^[46] and the modification to EPOCH by Charpin et al.^[41]. To easily account for arbitrary target structures, we define the shape of the optical region at the same place where particle species are initialized. There has been work including nonlinear optical effects in PIC or FDTD simulations^[36,59], although those effects are not considered here.

3. Simulation Setup

We begin by applying this simulation framework to a slab of fused silica (SiO_2) corresponding to the experiment discussed in Chimier et al.^[16] and then apply the framework to a multi-layer mirror as shown in Fig. 1. We test a range of fluences near the reported damage threshold, where the fluence is given by $F = 2E_{\text{las}}/\pi\omega_0^2$, with E_{las} being the energy of the laser pulse. The laser is introduced as a boundary condition and enters into vacuum before interacting with a slab of fused silica at normal incidence. For both the bulk and multi-layer targets, a $\lambda = 800 \text{ nm}$, $\tau_{\text{FWHM}} = 7 \text{ fs}$ pulse duration, sine-squared pulse with a spot radius of $\omega_0 = 4.65 \text{ }\mu\text{m}$ is modeled.

3.1. Grid and Particle Initialization

The simulation setup for bulk SiO_2 is shown in Fig. 1(a). The simulation box is $1.0 \text{ }\mu\text{m}$ in the longitudinal (y) direction and $9.6 \text{ }\mu\text{m}$ in the transverse (x/z) directions. The target is $0.9 \text{ }\mu\text{m}$ thick, leaving $0.1 \text{ }\mu\text{m}$ vacuum region before the laser interacts with the target. Simple outflow boundaries are used to allow transmission of the laser out of the simulation box with minimal reflection. The bulk silica simulations have a resolution of 5 nm in the longitudinal (y) direction and 40 nm in the transverse directions. A higher resolution was used in the longitudinal direction to better resolve the ionization dynamics at the interface between the target surface and the vacuum region.

¹with the exception of the elliptic integrals which are read from tabulated data files with 1,000 points

²<https://epochpic.github.io/>

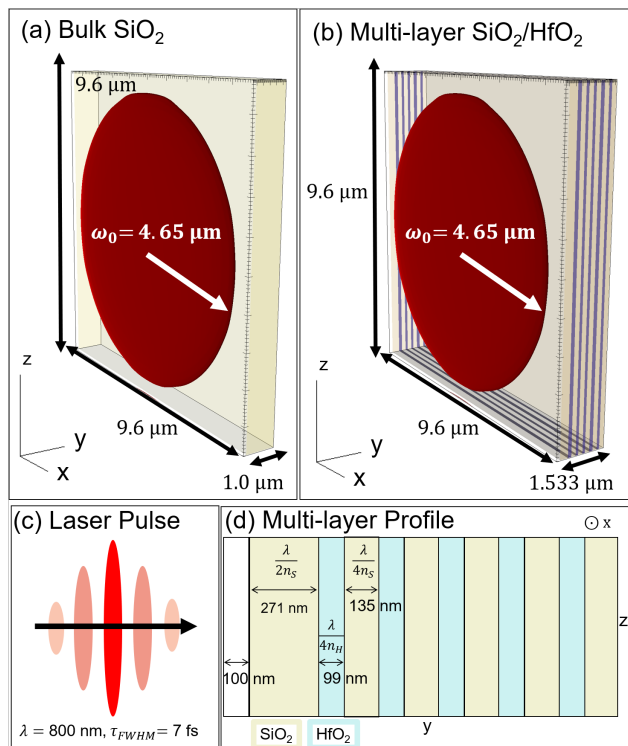


Figure 1. A schematic of the 3D simulations for bulk fused silica (a), and the coating of the multi-layer quarter-wave mirror with a fused SiO₂ protective layer (b). The normally incident few-cycle laser pulse (c) is driven from the minimum y boundary into a $0.1 \mu\text{m}$ vacuum region before the target. The SiO₂ regions are represented in yellow and the HfO₂ in blue. A cross section of the multi-layer mirror in the $x-z$ plane is shown in (d) (z dimension is not to scale). The thickness of the top SiO₂ layer is 270.90 nm and then there are alternating layers of HfO₂ (98.95 nm) and SiO₂ (135.45 nm).

Then we apply this framework to multi-layer interference coatings composed of alternating fused SiO₂ (yellow) and HfO₂ (blue) layers as shown in Fig. 1(b,d). The simulation space is $9.6 \mu\text{m}$ by $1.533 \mu\text{m}$ by $9.6 \mu\text{m}$ long in x , y , z respectively, with a resolution of 13.8 nm in the longitudinal (y) direction and 40 nm in the transverse directions. The thickness of the surface protective SiO₂ layer is $\lambda/(2n)$, while the rest of the layer thickness is $\lambda/(4n)$, a typical Bragg quarter-wavelength mirror, where n is the index of refraction for each material. The top fused SiO₂ layer is placed at $0 \mu\text{m}$ and the pulse enters normally from y -axis at $-0.1 \mu\text{m}$.

Both series of simulations are initialized with 1000 neutral SiO₂ (or HfO₂) macroparticles per cell with a temperature of 300 K . Similar to Charpin et al.^[41], we found that a large number of particles per cell were required for accuracy with the Keldysh ionization model in this regime. The simulations are run to a simulation time of 24 fs , which allows the pulse to make multiple passes across the simulation domain. For each simulation, we use the default time step in EPOCH of 0.95 times the Courant–Friedrichs–Lewy (CFL) limit^[60,61], or $0.95/(c\sqrt{1/\Delta x^2 + 1/\Delta y^2 + 1/\Delta z^2})$, where $\Delta x, y, z$ represents the grid size in each simulation dimension^[31].

3.2. Material Properties

The simulations require a number of material properties as inputs to model the interaction and interpret the predictions. These include the linear refractive index, density, and band gap, for which we use standard values listed in Table 1. There is less agreement in reported values for the effective electron and hole masses (m_e^* and m_h^* respectively) and subsequently this results in different reduced effective masses $m^* = 1/(1/m_e^* + 1/m_h^*)$. This variation leads to significant differences in predictions for the excited electron density using the Keldysh ionization model^[27,62]. To calculate m_e^* for fused HfO₂, we assume it is the spherically averaged effective mass around the Γ and B point of the monoclinic HfO₂^[63,64]. We generally use material properties for m-HfO₂ as those for amorphous HfO₂ are less readily available. These effective electron masses are used for ionized electron particles in the simulations.

4. Damage Modeling of Bulk Silica Target

We benchmark our framework against the experiment in Chimier et al.^{[16][21]}, which finds damage with a fluence of 1.18 J cm^{-2} and ablation at 1.3 J cm^{-2} for a 7 fs FWHM pulse at normal incidence. There is some uncertainty in these thresholds. Other experiments of LIDT for bulk silica with different experimental conditions including a shorter 5 fs pulses^[15,18] report thresholds from 1.5 to 1.8 J cm^{-2} . We use a $4.65 \mu\text{m}$ spot radius in our simulations to match the experimental conditions in Chimier et al.^[16]. We note that experiments by Lenzner et al.^[15] and Kafka et al.^[18] used

Table 1. Material Properties used in simulations.

Material	Band Gap (eV)	Index n	Density (g cm ⁻³)	m_p^*	m_e^*
SiO ₂	9 ^[26]	1.477	2.2 ^[65]	8 ^[66]	0.6 ^[66]
HfO ₂	5.7 ^[64]	2.021	9.68	1.12 ^[64]	1.09 ^[64]

larger spot sizes, although petawatt-class laser systems^[67] can often achieve spot sizes on the order of a few wavelengths (e.g., see Poole et al.^[68]).

4.1. Electron Density

For simulation and theoretical work, the predicted excited electron density is often used as a criterion to predict damage. Many studies use the critical electron density^[69] for free electrons or some fraction of total ionization^[70]. This qualitatively makes sense, as exceeding such thresholds can result in high absorption and subsequent damage. This choice has shown good agreement with longer pulses, although recent work has suggested that this description is insufficient for modeling shorter few-cycle pulses^[16,71]. As shown in Fig. 2, the damage threshold is predicted at about 0.8 J cm⁻² by the critical density criterion, which is about a 30% underestimation of the experimental LIDT. Number density is a standard output variable for PIC simulations. It is calculated by mapping the position of the macroparticles to the spatial grid based on the shape function selected for the simulation^[29-31].

Alternatively, the instability density suggested by Stampfli and Bennemann^[72] states that when the conduction band electron density reaches about 9% of the valence band electron density, the elastic shear constant will become negative and the lattice becomes unstable, which then leads directly to a very rapid melting of the crystal structure. This criterion was developed for crystals, but the fundamental physical principles—namely, the relationship between conduction band electron density and the stability of the atomic structure is similar. By applying this criterion to the bulk fused SiO₂ simulations, the damage is achieved at about 1.2 J cm⁻², which agrees with the experimental results.

4.2. Energy Density

The excited electron energy density criterion has also been suggested to predict damage^[71,73]. The predicted energy density is typically compared to material properties such as the dissociation energy, or an energy barrier associated with melting, or boiling^[71,74]. We compare the energy densities in our simulations to these thresholds.

Previous computational approaches typically assume some simple electron energy distribution, whereas in PIC, the energy density can be calculated directly with standard outputs. For our simulations, we multiply the number density by average particle energy for a species in each cell. Alternately, this could be re-sampled to a finer or a coarser

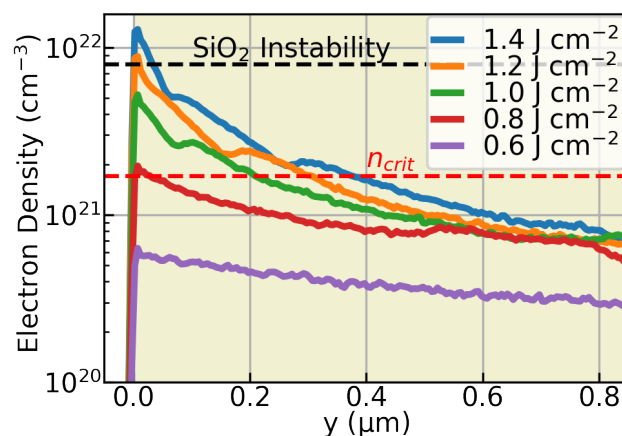


Figure 2. The electron density at the center of the x-z plane (Averaged over 6 cells in x and y) along y at 20 fs for a series of PIC simulations at various laser fluences with a 7 fs duration pulse interacting with bulk SiO₂. The critical plasma density n_{crit} and electron instability density from Stampfli and Bennemann^[72] are labeled with dashed lines. The latter predicts damage around 1.2 J cm⁻².

grid if the individual macroparticle positions and energies are extracted from the simulation.

Due to variations of reported material properties in the literature and uncertainty of previous simulations, the exact energy density for damage is not agreed upon. For reference, the dissociation energy of SiO₂ has reported values from 54–68 kJ cm⁻³ (Refs.^[73,75,76]). For comparison, the threshold for high energy density physics^[77] is ~ 100 kJ cm⁻³.

The energy densities related to melting or boiling are lower, where we can use the temperature-dependent heat capacity and latent heat of vaporization used in Zhao et al.^[78,79] to calculate an energy density of 5.7 kJ cm⁻³ for melting and 34.7 kJ cm⁻³ for boiling. We do have uncertainty in these values. The latent heat of vaporization has the largest contribution to the boiling criteria and there is a great deal of uncertainty in reported values. For example, the calculation above uses values from Bäuerle^[80] who calculate the latent heat of vaporization of c-SiO₂ to be 1.23×10^7 J kg⁻¹, while Kraus et al.^[81] report $1.177 \pm 0.095 \times 10^7$ J kg⁻¹, and Khmyrov et al.^[82] use 0.96×10^7 J kg⁻¹ (from Refs.^[83,84]). This gives a range from 28.7 kJ cm⁻³ to 35.6 kJ cm⁻³ for boiling. We expect some uncertainty in melting energy density as well.

Figure 3 shows the maximum energy density in simulations with and without collisions for a range of laser fluences. The simulations just including photoionization, (without collisions) have lower energy density at the end of

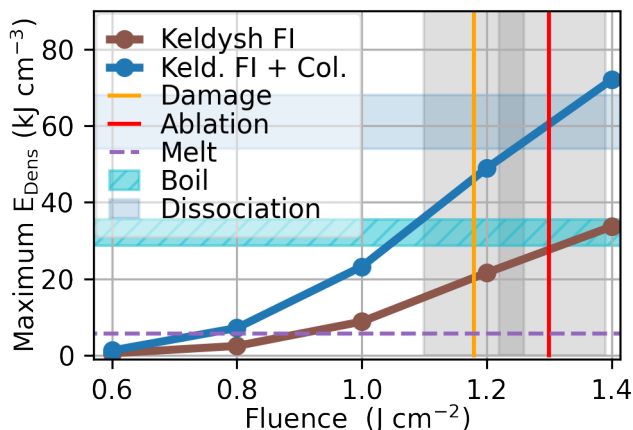


Figure 3. The peak energy density for the series of PIC simulations at various fluences with a 7 fs duration pulse interacting with bulk fused silica. The experiment^[16] being modeled observed damage around 1.18 J cm^{-2} and ablation^[21] at 1.3 J cm^{-2} . The shaded horizontal line/bands indicate approximate energy density thresholds for melting, boiling, and dissociation. The shaded vertical bands represent uncertainty in experimental damage and ablation thresholds. The simulations including collisions have a higher predicted energy density. Including both our Keldysh photoionization model and collisional effects show agreement between the expected damage fluence and the dissociation energy.

the simulation and do not exceed the boiling criterion until much higher fluences than are expected for LIDT in these conditions.

In Fig. 3, we see that at 1.3 J cm^{-2} , where ablation is observed in experiments, the simulation energy density overlaps with the reported dissociation energy values. For 1.2 J cm^{-2} near the LIDT, the energy density for the simulation is around 49 kJ cm^{-3} , exceeding the boiling threshold and near the dissociation energy.

4.3. Kinetic Particle Motion

The kinetic nature of PIC simulations allows us to explore the energy and motion of the excited electrons. While most previous approaches assume a thermal distribution of the excited electrons, Fig. 4, shows that this is not the case during the interaction. The spectra at different times of the simulation are shown and the energy is fitted by the χ^2 distribution using the SciPy^[85] library

$$\chi^2 : f(E_e; k, \sigma) = \frac{E_e^{k/2-1} e^{-\frac{E_e}{2\sigma}}}{(2\sigma)^{k/2} \Gamma(\frac{k}{2})}, \quad (5)$$

where E_e is the energy of the electrons, and fitting parameters k , σ are the degree and scale parameter, respectively. The χ^2 distribution becomes the standard Maxwell-Boltzmann distribution when $k=3$ and $\sigma=k_b T/2$. In our analysis, we primarily focus on the variation of the degrees of freedom k as it is crucial in describing the main characteristics of the Maxwell-Boltzmann distribution. For both cases, with or without collisions, the excited electrons are

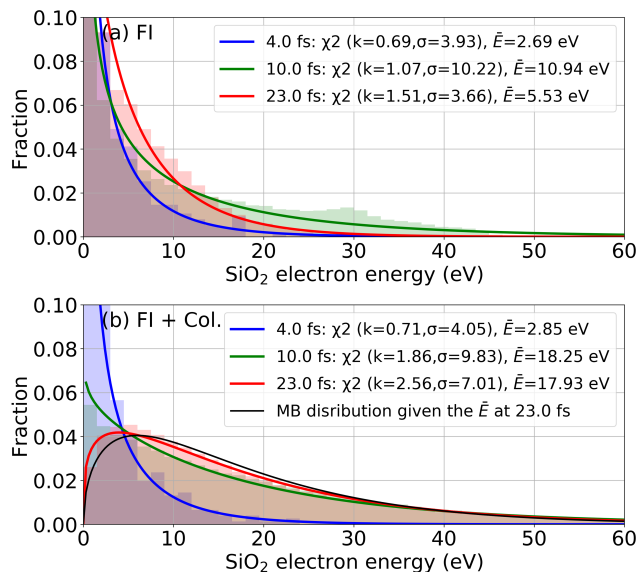


Figure 4. Excited electron energy distributions in a $(200 \text{ nm})^2 \times (900 \text{ nm})$ region of the target at the center of the interaction for a 1.2 J cm^{-2} pulse. A simulation with just field ionization is shown in (a) and a simulation with field ionization and collisions is shown in (b). A fit with the given temperature is shown. We observe the nonthermal nature, especially for early times and for simulations without collisions.

highly nonthermal at the early stage of 4 fs, the degree k is about 0.7. Then at 10 fs, after the peak intensity passed through the target, the energy spectrum is still nonthermal with $k=1.07$ when collision are not included, as shown in Fig. 4(a), while in Fig. 4(b) the degree k goes to 1.86. At the stable stage of 23 fs, the electrons still remain nonthermal in Fig. 4(a), while in Fig. 4(b), the k is about 2.56, which is approaching to the Maxwell-Boltzmann distribution as indicated by the black curve given the average energy at 23 fs. Therefore, our simulations not only show the dynamic evolution of the excited electron energy spectrum during the interaction, but also show the importance of including collisions to capture particle dynamics. When collisions are included in the simulations, the energy absorbed by the electrons increases, leading to a higher average energy (Fig. 4) and higher maximum energy density (Fig. 3) at the end of the simulation.

5. Damage Modeling of Multi-layer Mirrors

For the multi-layer dielectric mirror, HfO_2 is expected to have a lower damage threshold than SiO_2 ^[86,87] due to the lower bandgap. Therefore, the damage may be initiated in the first HfO_2 layer. For example, Talisa et al.^[22] found the damage threshold for a four-layer $\text{SiO}_2/\text{HfO}_2$ mirror to be half that of a bulk SiO_2 target. Due to the high computational cost of 3D simulations and uncertainty in material properties for HfO_2 , we explore a simple mirror with a relatively small spot size to gain a better qualitative understanding of the interaction. Future validations with experiment should be

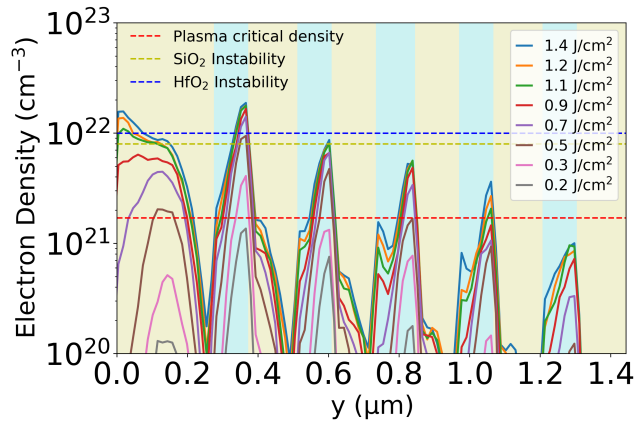


Figure 5. The electron density at the center of the x - z plane along y at 20 fs for a series of PIC simulations at various fluences with a 7 fs duration pulse interacting with multi-layer mirror. The yellow area is SiO_2 , and blue area is HfO_2 . Different critical electron densities are labeled in the figure with dashed lines.

coupled with more accurate material property measurements and LIDT measurements of bulk HfO_2 .

5.1. Electron Density

As mentioned in Sec. 4, the plasma critical density may underestimate the damage threshold, it predicts the LIDT slightly above 0.2 J cm^{-2} in the first HfO_2 layer as shown in Fig. 5. If we apply the instability density criterion to the mirror target, the damage may be achieved at about 0.5 J cm^{-2} in the same layer. Above 0.7 J cm^{-2} , the hot spots in the top two layers are almost fully ionized as the peak electron density reaches about $1.5 \times 10^{22} \text{ cm}^{-3}$.

5.2. Energy Density

The peak electron energy density along y at the center of x - z plane in each layer with different fluences is shown in Fig. 6. The dissociation energy of fused HfO_2 has not been extensively studied, particularly for amorphous samples, which are expected in these multi-layer coatings. There are reported values for the formation energy density of $m\text{-HfO}_2$ from 48.44 to 52.64 kJ cm^{-3} [88–94], which are similar to the dissociation energy density of SiO_2 . We assume it has the same value as fused SiO_2 since both of their molecules have four valence band electrons and are amorphous [281], which is about 54 kJ cm^{-3} indicated by the red dashed line. In addition, the effects of structure on boiling and melting points are not considered, as each layer is assumed to retain the melting and boiling points characteristic of its bulk state. This criterion suggests the damage should occur at the surface at fluence of about 1.4 J cm^{-2} , which is even higher than the LIDT of bulk fused SiO_2 discussed in Sec. 4.

Instead let us consider energy density thresholds for melting and boiling as these may relate to damage within the layers of a coating. To calculate the melting and boiling

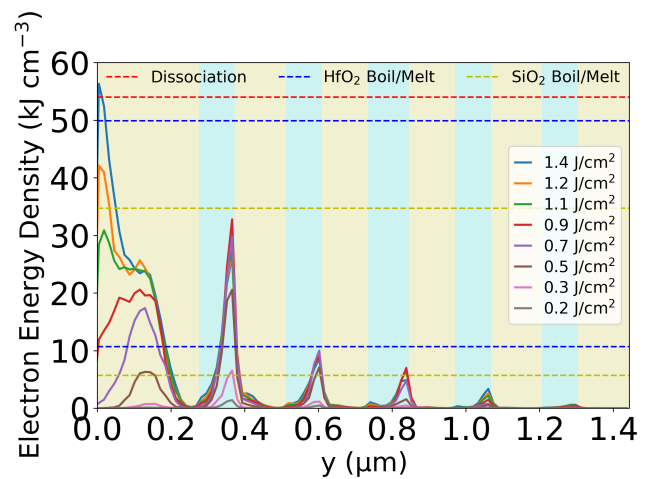


Figure 6. The peak electron energy density at the center of x - z plane along y at 20 fs for a series of PIC simulations at various fluences with a 7 fs duration pulse interacting with multi-layer mirror. The yellow area is fused SiO_2 , and blue area is fused HfO_2 . The SiO_2 boiling and melting energy density are at about 34.7 kJ cm^{-3} and 5.7 kJ cm^{-3} indicated as the yellow dashed lines, and the HfO_2 boiling and melting energy density are at about 49.9 kJ cm^{-3} and 10.7 kJ cm^{-3} indicated as the blue dashed lines.

energy densities, we make the following assumptions: (a) the vaporization latent heat for HfO_2 is the same as SiO_2 , and (b) the heat capacity for fused HfO_2 is the same as $m\text{-HfO}_2$ [95]. These approximations give the boiling energy density of HfO_2 to be about 49.9 kJ cm^{-3} , which is much higher than that of SiO_2 34.7 kJ cm^{-3} , and may overestimate the actual damage threshold. Similarly, the melting energy density of SiO_2 is about 5.7 kJ cm^{-3} , and we calculated about 10.7 kJ cm^{-3} for HfO_2 .

The boiling energy density criterion predicts LIDT at a fluence between 1.1 J cm^{-2} and 1.2 J cm^{-2} on the surface of the mirror, which is close to the LIDT of bulk SiO_2 . Alternately, applying the melting energy density criterion gives the LIDT to be less than 0.5 J cm^{-2} , and the damage site is initiated in the first HfO_2 layer as expected.

5.3. Plasma Screening Effects

As shown in Fig. 6, the global maximum energy density at low fluences is in the first HfO_2 layer as expected. When the fluence exceeds about 1.1 J cm^{-2} it shifts to the top SiO_2 layer and the HfO_2 energy density increases slowly after the fluence reaches about 0.7 J cm^{-2} . This is because the excited electron density in the first SiO_2 layer begins to exceed the critical plasma density (Fig. 5). In the top SiO_2 layer, the steady state of the dynamic simulation leads to a local maximum enhancement of the electric field at the center.

As the fluence increases beyond 0.5 J cm^{-2} , we observe a new peak appearing and shifting from the center to the surface in both the electron and energy density profiles. The ionization rate at the center of the top SiO_2 layer is enhanced

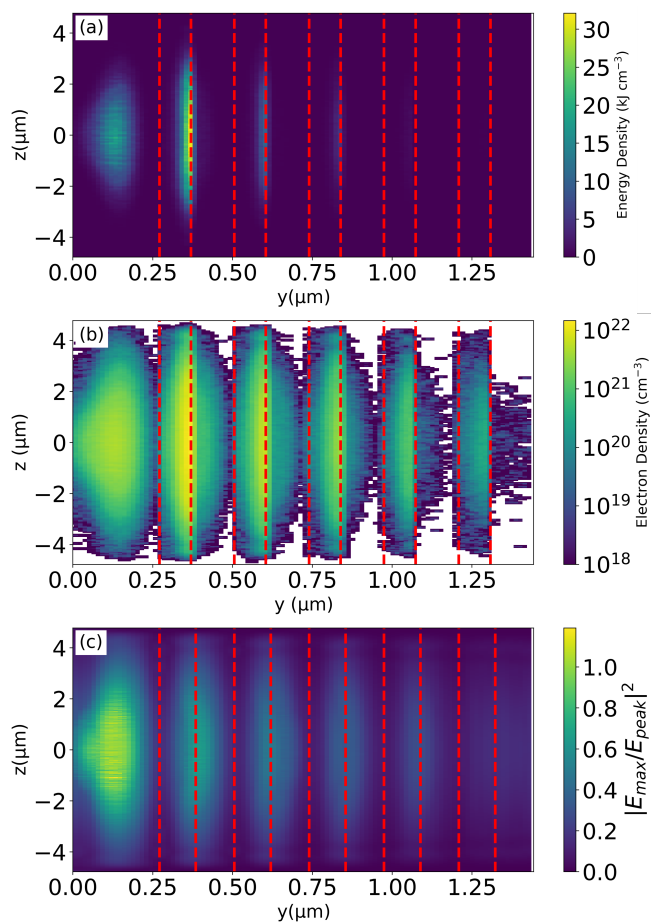


Figure 7. The (a) energy density and (b) electron density at the center of x on y - z plane at 20 fs at 0.7 J cm^{-2} with a 7 fs duration pulse interacting with multi-layer mirror. The mirror surface starts at $y=0$, and the dashed red lines are the interfaces between layers. The white areas have no excited electrons. (c) The maximum accumulated normalized intensity over the entire simulation.

due to the strong intensity and thus the electron density reaches a maximum. The absorption and reflection will continue to increase so that the source can hardly penetrate the target by the end of the laser pulse. Therefore, the resonant pattern of the electric field is altered, and a new intensity peak appears.

To illustrate this process clearly, a two-dimensional y - z cross section of the layers at the center of x -axis are shown in Fig. 7 at fluence of 0.7 J cm^{-2} . The maximum electron and energy density are both observed in the first HfO_2 layer as shown in (a) and (b), while the maximum accumulated intensity is in the first SiO_2 layer in (c). The intensity is recorded at intervals of 0.5 fs and compared across all time points to generate this figure. These results are similar to those from FDTD simulations by Zhang et al.^[28].

Noticeably, the electron, energy density, and intensity profiles in the protective SiO_2 layer all present a bump extending from the center to the surface, which is different from what previous FDTD simulation works by Zhang

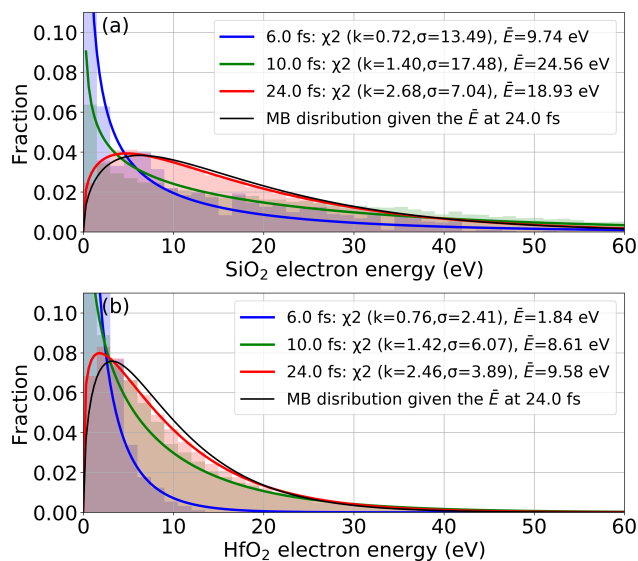


Figure 8. The energy histogram for the electrons in the first SiO_2 layer (a) and HfO_2 layer (b) at 6, 10, 24 fs for the 0.7 J cm^{-2} simulation with χ^2 distribution fitted. The black curve is the Maxwell-Boltzmann distribution given the average energy at the stable stage around 24 fs.

et al.^[28]. We observed that the electron density peak first appeared at the center and then expanded at about 9 fs to the surface, and became stable at about 15 fs. These are the times when the pulse peak intensity reached the surface and when the entire pulse left the surface.

Furthermore, in Fig. 6, the first HfO_2 layer is more strongly affected by the lower fluence pulse. At higher fluence, there is significant growth of the energy density at the surface, while the lower layers do not show as significant of an increase. In addition, the energy density at 0.9 J cm^{-2} is highest among all the fluences, which adds additional evidence that the first SiO_2 layer has reflected more injected energy due to the plasma screening effects.

The plasma generation could also imply the breakdown threshold which is defined as a permanent change to the optical properties. We can see from both energy and electron density profiles, the local peak in the top SiO_2 layer starts to shift at 0.5 J cm^{-2} and the profile is no longer symmetric at the center. This analysis is also consistent with the conclusion predicted by the instability criterion.

5.4. Particle Energy

The kinetic nature of the excited electrons is shown in Fig. 8. The spectrum of the electrons in the SiO_2 layer is wider than that in the HfO_2 layer, though both maximum electron density and energy density reaches maximum in the first HfO_2 layer. For both layers, three snapshots of the energy distribution are shown. At 6 fs, in the early stage of the interaction, there are some excited electrons generated from the ionization. The electrons are highly nonthermalized since the degree k is less than one. At about 10 fs, the peak

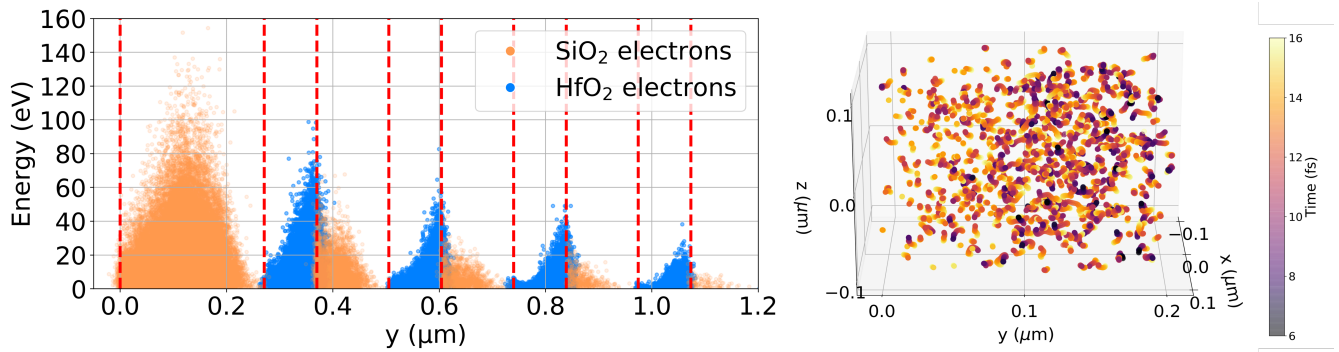


Figure 9. The SiO₂ and HfO₂ electron energy spatial distribution for a fluence of 0.7 J cm^{-2} is shown on the left at 24 fs. The highest energy particles are found in the center of the first layer and at the interfaces between layers. Particle trajectories for a random 2% of electrons with low (below average) final energy demonstrate the ionization dynamics in the first SiO₂ layer up to 16 fs (after the pulse has left). Ionization near the surface generally occurs at later times as indicated by the color of the tracks.

intensity has passed through the target, leading to an average electron energy of 24.56 eV and 8.61 eV for the SiO₂ and HfO₂ layers. The electrons are still nonthermalized as k is about 1.4. At 24 fs, the pulse front has left the target for about 10 fs. The degree k is above 2 and approaching to 3, indicating the thermalization process is finishing towards a Maxwell-Boltzmann distribution indicated by the black curves in Fig. 8.

5.5. Particle Dynamics

The peak intensity of the 0.7 J cm^{-2} pulse is about $10^{14} \text{ W cm}^{-2}$, giving a theoretical ponderomotive energy^[96] U_p of approximately 10 eV and 5.5 eV for SiO₂ and HfO₂ electrons respectively (using the m_e^* values from Table 1). Some studies have reported keV-scale electron spectra under similar intensities but with longer pulse durations^[96]. This enhancement is often attributed to the surface modification of the target due to ablation, which enhances the local intensity and facilitates stronger electron acceleration. In our previous work, we also observed keV-scale spectra using a 7 fs pulse by introducing pit-like defects on the target surface under comparable conditions^[40].

In gases, electrons with kinetic energies exceeding $10U_p$ are typically observed^[97], and in our simulation, the highest electron energy from the first SiO₂ layer reaches up to 150 eV. Additionally, a few electrons in the first HfO₂ layer achieve energies around 100 eV, as shown in Fig. 9 (left). These results align with the kinetic energy predictions for excited electrons based on the Drude model. If we assume the collisional frequency is 1 fs^{-1} , then the energy would be about 118 eV and 65 eV for SiO₂ and HfO₂, as seen in the studies by Duchateau et al.^[98] Furthermore, the excited SiO₂ electrons at the HfO₂-SiO₂ interfaces rarely enter the HfO₂ layers. There are a limited number of HfO₂ electrons penetrating into the adjacent SiO₂ layers for a few tens of nanometers.

The tracks of select electrons in the first SiO₂ layer are

shown from 6 to 16 fs in Fig. 9 (right). Most electrons near the vacuum interface are born after 10 fs, indicated by their yellowish tails. In contrast, electrons near the center of the first SiO₂ layer are born earlier. This suggests that the electron density expansion in Fig. 5 and Fig. 7(b) is due to direct excitation near the surface rather than displacement from the center.

6. Conclusion

Understanding few-cycle pulse interactions with dielectric optical components and their LIDT is essential for advancing next-generation laser systems. The use of kinetic simulations in relevant regimes are becoming increasingly popular^[33,36,37,41]. Kinetic simulations allow us to capture the nonthermal nature of the initial interaction, which is important to accurately model absorption and ionization. We show that both excited electron density and energy density provide insight into LIDT. Our framework shows good agreement with experimental LIDTs for bulk silica targets. Multi-layer mirror simulations indicate that plasma screening effects can alter the laser interaction and electron energy distribution for high fluences.

In the future, this framework can be applied to a variety of mirror and grating designs^[28] for both near and mid-infrared wavelengths^[39,99]. Additionally, simulations can be inserted into an optimization algorithm to optimize LIDT or other properties of interest for optical components^[100]. This framework already provides a deeper qualitative understanding of the dynamics of laser damage, and we show promising quantitative agreement with experiment for few-cycle pulses. Further development of this framework including impact ionization^[41,54], coupled with more precise measurements of material properties for relevant optical coating designs can allow further validation of the framework across large ranges of laser fluence.

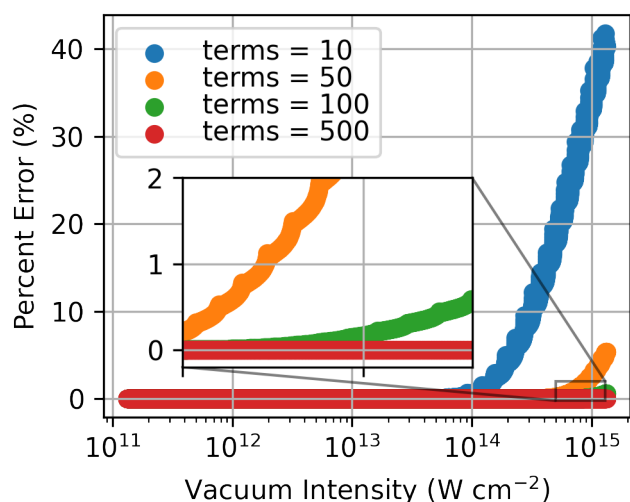


Figure 10. Percent error for 10 to 500 terms in the infinite sum in Eq. 3 for SiO₂ at varying laser intensities. The error is calculated with the result for 1,000 terms as the ‘actual’ value. Our simulation framework uses 500 terms, which shows a negligible difference compared to 1,000 terms for these intensities. The errors for HfO₂ (not shown) are of similar magnitude to those for SiO₂.

A. Keldysh Ionization Model Implementation

Here we include additional implementation details for our Keldysh ionization model in EPOCH. As stated in Sec. 2.1, we use 500 terms in the infinite sum in Eq. 3. To decide the number of terms, we tested the convergence as shown in Fig. 10. Using 100 terms yields errors below 1% for our laser intensities, while selecting 500 terms provided results nearly identical to 1,000 terms.

The Dawson integral (\mathcal{D} in Eq. 3) is evaluated using John Burkardt’s Fortran 90 code^[101], which is based on the work by Cody et al.^[102].

Acknowledgements

This research was funded by DOE STTR grant no. DE-SC0019900. This research used resources of the National Energy Research Scientific Computing Center (NERSC), a Department of Energy Office of Science User Facility using NERSC award SBIR-ERCAP0021422. This project also utilized resources from the Ohio Supercomputer Center^[103]. The code EPOCH used in this work was in part funded by the UK EPSRC grants EP/G054950/1, EP/G056803/1, EP/G055165/1 and EP/M022463/1. This work used matplotlib^[104], SciPy^[85], and NumPy^[105] to graph and analyze the simulation results.

References

1. The Royal Swedish Academy of Sciences. The Nobel prize in physics 2023. <https://www.nobelprize.org/prizes/physics/2023/press-release/>, 2023. Accessed: (08/06/2024).
2. National Academies of Sciences Engineering and Medicine. *Opportunities in Intense Ultrafast Lasers: Reaching for the Brightest Light*. National Academies Press, 2018. doi: <https://doi.org/10.17226/24939>.
3. Roger Falcone, Félicie Albert, Farhat Beg, Siegfried Glenzer, Todd Ditmire, Tom Spinka, and Jonathan Zuegel. Workshop report: Brightest light initiative (March 27-29 2019, OSA headquarters, Washington, D.C.), 2 2020. URL <https://www.osti.gov/biblio/1604161>.
4. M Ferray, Anne L’Huillier, XF Li, LA Lompre, G Mainfray, and C Manus. Multiple-harmonic conversion of 1064 nm radiation in rare gases. *Journal of Physics B: Atomic, Molecular and Optical Physics*, 21(3):L31, 1988. doi: 10.1088/0953-4075/21/3/001. URL <https://dx.doi.org/10.1088/0953-4075/21/3/001>.
5. Pierre-Marie Paul, Elena S Toma, Pierre Breger, Genevive Mullot, Frédérique Augé, Ph Balcou, Harm Geert Muller, and Pierre Agostini. Observation of a train of attosecond pulses from high harmonic generation. *Science*, 292(5522):1689–1692, 2001. URL <https://doi.org/10.1126/science.1059413>.
6. Michael Hentschel, Reinhard Kienberger, Ch Spielmann, Georg A Reider, Nenad Milosevic, Thomas Brabec, Paul Corkum, Ulrich Heinzmann, Markus Drescher, and Ferenc Krausz. Attosecond metrology. *Nature*, 414(6863):509–513, 2001. URL <https://doi.org/10.1038/35107000>.
7. Thomas Brabec and Ferenc Krausz. Intense few-cycle laser fields: Frontiers of nonlinear optics. *Rev. Mod. Phys.*, 72:545–591, Apr 2000. doi: 10.1103/RevModPhys.72.545. URL <https://link.aps.org/doi/10.1103/RevModPhys.72.545>.
8. Tamas Nagy, Peter Simon, and Laszlo Veisz. High-energy few-cycle pulses: post-compression techniques. *Advances in Physics: X*, 6(1):1845795, 2021. doi: 10.1080/23746149.2020.1845795. URL <https://doi.org/10.1080/23746149.2020.1845795>.
9. Tibor Wittmann, Balint Horvath, Wolfram Helml, Michael G Schätzel, Xun Gu, Adrian L Cavalieri, GG Paulus, and Reinhard Kienberger. Single-shot carrier-envelope phase measurement of few-cycle laser pulses. *Nature Physics*, 5(5):357–362, 2009. doi: 10.1364/OPTICA.7.000035. URL <https://opg.optica.org/optica/abstract.cfm?URI=optica-7-1-35>.
10. F. Mackenroth, A. Di Piazza, and C. H. Keitel. Determining the carrier-envelope phase of intense few-cycle laser pulses. *Phys. Rev. Lett.*, 105:063903, Aug 2010. doi: 10.1103/PhysRevLett.105.063903. URL <https://link.aps.org/doi/10.1103/PhysRevLett.105.063903>.
11. Julius Huijts, Igor A Andriyash, Lucas Rovige, Aline

- Vernier, and Jérôme Faure. Identifying observable carrier-envelope phase effects in laser wakefield acceleration with near-single-cycle pulses. *Physics of Plasmas*, 28(4), 2021. doi: 10.1063/5.0037925. URL <https://doi.org/10.1063/5.0037925>.
12. Antoine Cavagna, Milo Eder, Enam Chowdhury, André Kalouguine, Jaismeen Kaur, Gérard Mourou, Stefan Haessler, and Rodrigo Lopez-Martens. Continuous relativistic high-harmonic generation from a kHz liquid-sheet plasma mirror. *Opt. Lett.*, 50(1):165–168, Jan 2025. doi: 10.1364/OL.545912. URL <https://opg.optica.org/ol/abstract.cfm?URI=ol-50-1-165>.
 13. B. C. Stuart, M. D. Feit, S. Herman, A. M. Rubenchik, B. W. Shore, and M. D. Perry. Optical ablation by high-power short-pulse lasers. *J. Opt. Soc. Am. B*, 13(2):459–468, Feb 1996. doi: 10.1364/JOSAB.13.000459. URL <http://opg.optica.org/josab/abstract.cfm?URI=josab-13-2-459>.
 14. D. Du, X. Liu, G. Korn, J. Squier, and G. Mourou. Laser-induced breakdown by impact ionization in SiO₂ with pulse widths from 7 ns to 150 fs. *Applied Physics Letters*, 64(23):3071–3073, 06 1994. ISSN 0003-6951. doi: 10.1063/1.111350. URL <https://doi.org/10.1063/1.111350>.
 15. M. Lenzner, J. Krüger, S. Sartania, Z. Cheng, Ch. Spielmann, G. Mourou, W. Kautek, and F. Krausz. Femtosecond optical breakdown in dielectrics. *Phys. Rev. Lett.*, 80:4076–4079, May 1998. doi: 10.1103/PhysRevLett.80.4076. URL <https://link.aps.org/doi/10.1103/PhysRevLett.80.4076>.
 16. B. Chimier et al. Damage and ablation thresholds of fused-silica in femtosecond regime. *Phys. Rev. B*, 84:094104, Sep 2011. doi: 10.1103/PhysRevB.84.094104. URL <https://link.aps.org/doi/10.1103/PhysRevB.84.094104>.
 17. Matthias Lenzner, J Krüger, Wolfgang Kautek, and Ferenc Krausz. Precision laser ablation of dielectrics in the 10-fs regime. *Applied Physics A: Materials Science & Processing*, 68(3), 1999. doi: <https://doi.org/10.1007/s003390050906>.
 18. Kyle R. P. Kafka, Noah Talisa, Gabriel Tempea, Drake R. Austin, Catalin Neacsu, and Enam A. Chowdhury. Few-cycle pulse laser induced damage threshold determination of ultra-broadband optics. *Opt. Express*, 24(25):28858–28868, Dec 2016. doi: 10.1364/OE.24.028858. URL <http://opg.optica.org/oe/abstract.cfm?URI=oe-24-25-28858>.
 19. N. Sanner, O. Utéza, B. Chimier, M. Sentis, P. Lassonde, F. Légaré, and J. C. Kieffer. Toward determinism in surface damaging of dielectrics using few-cycle laser pulses. *Applied Physics Letters*, 96(7):071111, 02 2010. ISSN 0003-6951. doi: 10.1063/1.3309700. URL <https://doi.org/10.1063/1.3309700>.
 20. L. Hoffart, P. Lassonde, F. Légaré, F. Vidal, N. Sanner, O. Utéza, M. Sentis, J.-C. Kieffer, and I. Brunette. Surface ablation of corneal stroma with few-cycle laser pulses at 800 nm. *Opt. Express*, 19(1):230–240, Jan 2011. doi: 10.1364/OE.19.000230. URL <https://opg.optica.org/oe/abstract.cfm?URI=oe-19-1-230>.
 21. O Utéza, N Sanner, B Chimier, A Brocas, N Varkentina, M Sentis, P Lassonde, F Légaré, and JC Kieffer. Control of material removal of fused silica with single pulses of few optical cycles to sub-picosecond duration. *Applied Physics A*, 105:131–141, 2011. doi: 10.1007/s00339-011-6469-y.
 22. Noah Talisa, Abdallah Alshafey, Michael Tripepi, Jacob Krebs, Aaron Davenport, Emmett Randel, Carmen S. Menoni, and Enam A. Chowdhury. Comparison of damage and ablation dynamics of multilayer dielectric films initiated by few-cycle pulses versus longer femtosecond pulses. *Opt. Lett.*, 45(9):2672–2675, May 2020. doi: 10.1364/OL.389650. URL <https://opg.optica.org/ol/abstract.cfm?URI=ol-45-9-2672>.
 23. Maciej Kowalczyk, Nathalie Nagl, Philipp Steinleitner, Nicholas Karpowicz, Vladimir Pervak, Aleksander Głuszek, Arkadiusz Hudzikowski, Ferenc Krausz, Ka Fai Mak, and Alexander Weigel. Ultra-cep-stable single-cycle pulses at 2.2 μm . *Optica*, 10(6):801–811, Jun 2023. doi: 10.1364/OPTICA.481673. URL <https://opg.optica.org/optica/abstract.cfm?URI=optica-10-6-801>.
 24. Dandan Hui, Husain Alqattan, Simin Zhang, Vladimir Pervak, Enam Chowdhury, and Mohammed Th. Hassan. Ultrafast optical switching and data encoding on synthesized light fields. *Science Advances*, 9(8):eadf1015, 2023. doi: 10.1126/sciadv.adf1015. URL <https://www.science.org/doi/abs/10.1126/sciadv.adf1015>.
 25. Luca Argenti, Michael Chini, and Li Fang, editors. *Proceedings of the 8th International Conference on Attosecond Science and Technology*. Springer Nature, 2024. doi: <https://doi.org/10.1007/978-3-031-47938-0>.
 26. JR Peñano, P Sprangle, B Hafizi, W Manheimer, and A Zigler. Transmission of intense femtosecond laser pulses into dielectrics. *Physical Review E*, 72(3):036412, 2005. doi: 10.1103/PhysRevE.72.036412. URL <https://link.aps.org/doi/10.1103/PhysRevE.72.036412>.
 27. Simin Zhang, Aaron Davenport, Noah Talisa, Joseph R. Smith, Carmen S. Menoni, Vitaly E. Gruzdev, and Enam A. Chowdhury. 2D dynamic ionization simulation from ultrashort pulses in multilayer dielectric interference coatings. In Christopher Wren Carr, Vitaly E. Gruzdev, Detlev Ristau, and Carmen S. Menoni, editors, *Laser-induced Damage in Optical Materials 2020*, volume 11514,

- pages 74 – 83. International Society for Optics and Photonics, SPIE, 2020. doi: 10.1117/12.2571081. URL <https://doi.org/10.1117/12.2571081>.
28. Simin Zhang, Carmen Menoni, Vitaly Gruzdev, and Enam Chowdhury. Ultrafast laser material damage simulation—a new look at an old problem. *Nanomaterials*, 12(8):1259, 2022. URL <https://www.mdpi.com/2079-4991/12/8/1259>.
 29. C.K. Birdsall and A.B. Langdon. *Plasma Physics Via Computer Simulation*. Series In Plasma Physics. Taylor & Francis, 2004. ISBN 9780750310253. URL <https://doi.org/10.1201/9781315275048>.
 30. R Hockney and J Eastwood. *Computer simulations using particles*. crc Press, 1988. URL <https://doi.org/10.1201/9780367806934>.
 31. TD Arber, Keith Bennett, CS Brady, A Lawrence-Douglas, MG Ramsay, NJ Sircombe, P Gillies, RG Evans, Holger Schmitz, AR Bell, and Ridgers CP. Contemporary particle-in-cell approach to laser-plasma modelling. *Plasma Physics and Controlled Fusion*, 57(11):113001, 2015. doi: 10.1088/0741-3335/57/11/113001.
 32. Tim Ziegler, Ilja Göthel, Stefan Assenbaum, Constantin Bernert, Florian-Emanuel Brack, Thomas E Cowan, Nicholas P Dover, Lennart Gaus, Thomas Kluge, Stephan Kraft, et al. Laser-driven high-energy proton beams from cascaded acceleration regimes. *Nature Physics*, pages 1–6, 2024. URL <https://doi.org/10.1038/s41567-024-02505-0>.
 33. Robert A. Mitchell, Douglass W. Schumacher, and Enam A. Chowdhury. Modeling crater formation in femtosecond-pulse laser damage from basic principles. *Opt. Lett.*, 40(10):2189–2192, May 2015. doi: 10.1364/OL.40.002189. URL <http://opg.optica.org/ol/abstract.cfm?URI=ol-40-10-2189>.
 34. Ginevra E. Cochran, Patrick L. Poole, and Douglass W. Schumacher. Modeling pulse-cleaning plasma mirrors from dielectric response to saturation: A particle-in-cell approach. *Physics of Plasmas*, 26(10):103103, 2019. doi: 10.1063/1.5109683. URL <https://doi.org/10.1063/1.5109683>.
 35. P. B. Corkum. Plasma perspective on strong field multiphoton ionization. *Phys. Rev. Lett.*, 71:1994–1997, Sep 1993. doi: 10.1103/PhysRevLett.71.1994. URL <https://link.aps.org/doi/10.1103/PhysRevLett.71.1994>.
 36. Jean-Luc Déziel, Louis J. Dubé, Sandra H. Messaddeq, Younès Messaddeq, and Charles Varin. Femtosecond self-reconfiguration of laser-induced plasma patterns in dielectrics. *Phys. Rev. B*, 97:205116, May 2018. doi: 10.1103/PhysRevB.97.205116. URL <https://link.aps.org/doi/10.1103/PhysRevB.97.205116>.
 37. Wen Jun Ding, Jeremy Zhen Jie Lim, Hue Thi Bich Do, Xiao Xiong, Zackaria Mahfoud, Ching Eng Png, Michel Bosman, Lay Kee Ang, and Lin Wu. Particle simulation of plasmons. *Nanophotonics*, 9(10):3303–3313, 2020. doi: doi:10.1515/nanoph-2020-0067. URL <https://doi.org/10.1515/nanoph-2020-0067>.
 38. Hue Thi Bich Do, Ding Wen Jun, Zackaria Mahfoud, Wu Lin, and Michel Bosman. Electron dynamics in plasmons. *Nanoscale*, 13(5):2801–2810, 2021. URL <http://dx.doi.org/10.1039/D0NR07025D>.
 39. Maxim R Shcherbakov, Giovanni Sartorello, Simin Zhang, Joshua Bocanegra, Melissa Bosch, Michael Tripepi, Noah Talisa, Abdallah AlShafey, Joseph Smith, Stephen Londo, François Légaré, Enam Chowdhury, and Gennady Shvets. Nanoscale reshaping of resonant dielectric microstructures by light-driven explosions. *Nature communications*, 14(1):6688, 2023. URL <https://doi.org/10.1038/s41467-023-42263-w>.
 40. Joseph R Smith, Simin Zhang, Vitaly E Gruzdev, and Enam A Chowdhury. Intense few-cycle pulse, conical pit interaction simulations predicting extreme material states. In *2021 Conference on Lasers and Electro-Optics (CLEO)*, pages 1–2. IEEE, 2021. URL https://doi.org/10.1364/CLEO_SI.2021.SW4C.5.
 41. P-J Charpin, K Ardaneh, B Morel, R Giust, and F Courvoisier. Simulation of laser-induced ionization in wide bandgap solid dielectrics with a particle-in-cell code. *Optics Express*, 32(6):10175–10189, 2024. URL <https://doi.org/10.1364/OE.511590>.
 42. LV Keldysh. Ionization in the field of a strong electromagnetic wave. *JETP*, 20(5):1307–1314, 1965.
 43. Vitali E. Gruzdev. Analysis of Keldysh’s formula for the ionization rate in solids. In Mikhail N. Libenson, editor, *Nonresonant Laser-Matter Interaction (NLMI-11)*, volume 5506, pages 138 – 151. International Society for Optics and Photonics, SPIE, 2004. URL <https://doi.org/10.1117/12.580021>.
 44. Joseph R. Smith, Chris Orban, Nashad Rahman, Brendan McHugh, Ricky Oropeza, and Enam A. Chowdhury. A particle-in-cell code comparison for ion acceleration: EPOCH, LSP, and WarpX. *Physics of Plasmas*, 28(7):074505, 07 2021. ISSN 1070-664X. doi: 10.1063/5.0053109. URL <https://doi.org/10.1063/5.0053109>.
 45. Heiko Burau, Renée Widera, Wolfgang Hönig, Guido Juckeland, Alexander Debus, Thomas Kluge, Ulrich Schramm, Tomas E. Cowan, Roland Sauerbrey, and Michael Bussmann. PIConGPU: A fully relativistic particle-in-cell code for a GPU cluster. *IEEE Transactions on Plasma Science*, 38(10):2831–2839, 2010. doi: 10.1109/TPS.2010.2064310.
 46. Luca Fedeli, Axel Huebl, France Boillod-Cerneux, Thomas Clark, Kevin Gott, Conrad Hillairet, Stephan Jaure, Adrien Leblanc, Rémi Lehe, Andrew Myers, Christelle Piechurski, Mitsuhsa Sato, Neil Zaim,

- Weiqun Zhang, Jean-Luc Vay, and Henri Vincenti. Pushing the frontier in the design of laser-based electron accelerators with groundbreaking mesh-refined particle-in-cell simulations on exascale-class supercomputers. In *SC22: International Conference for High Performance Computing, Networking, Storage and Analysis*, pages 1–12, 2022. doi: 10.1109/SC41404.2022.00008.
47. Vitali E Gruzdev. Laser-induced ionization of solids: back to keldysh. In *Laser-Induced Damage in Optical Materials: 2004*, volume 5647, pages 480–492. SPIE, 2005. doi: <http://dx.doi.org/10.1117/12.578469>.
 48. An-Chun Tien, Sterling Backus, Henry Kapteyn, Margaret Murnane, and Gérard Mourou. Short-pulse laser damage in transparent materials as a function of pulse duration. *Phys. Rev. Lett.*, 82:3883–3886, May 1999. doi: 10.1103/PhysRevLett.82.3883. URL <https://link.aps.org/doi/10.1103/PhysRevLett.82.3883>.
 49. P Balling and Jørgen Schou. Femtosecond-laser ablation dynamics of dielectrics: basics and applications for thin films. *Reports on progress in physics*, 76(3):036502, 2013. URL <https://dx.doi.org/10.1088/0034-4885/76/3/036502>.
 50. Davide Terzani and Pasquale Londrillo. A fast and accurate numerical implementation of the envelope model for laser–plasma dynamics. *Computer Physics Communications*, 242:49–59, 2019. doi: <https://doi.org/10.1016/j.cpc.2019.04.007>.
 51. F. Pérez, L. Gremillet, A. Decoster, M. Drouin, and E. Lefebvre. Improved modeling of relativistic collisions and collisional ionization in particle-in-cell codes. *Physics of Plasmas*, 19(8):083104, 2012. doi: 10.1063/1.4742167. URL <https://doi.org/10.1063/1.4742167>.
 52. K. Nanbu and S. Yonemura. Weighted particles in coulomb collision simulations based on the theory of a cumulative scattering angle. *Journal of Computational Physics*, 145(2):639–654, 1998. ISSN 0021-9991. doi: <https://doi.org/10.1006/jcph.1998.6049>. URL <https://www.sciencedirect.com/science/article/pii/S0021999198960491>.
 53. Y. T. Lee and R. M. More. An electron conductivity model for dense plasmas. *The Physics of Fluids*, 27(5):1273–1286, 1984. doi: 10.1063/1.864744. URL <https://aip.scitation.org/doi/abs/10.1063/1.864744>.
 54. S. Morris, T. Goffrey, K. Bennett, and T. Arber. Improvements to collisional ionization models for particle-in-cell codes. *Physics of Plasmas*, 29(12):123907, 12 2022. ISSN 1070-664X. doi: 10.1063/5.0126336. URL <https://doi.org/10.1063/5.0126336>.
 55. LV Keldysh. Concerning the theory of impact ionization in semiconductors. *Sov. Phys. JETP*, 21(6):1135, 1965.
 56. Jean-Luc Déziel, Louis J. Dubé, and Charles Varin. Dynamical rate equation model for femtosecond laser-induced breakdown in dielectrics. *Phys. Rev. B*, 104:045201, Jul 2021. doi: 10.1103/PhysRevB.104.045201. URL <https://link.aps.org/doi/10.1103/PhysRevB.104.045201>.
 57. G M Petrov and J Davis. Interaction of intense ultra-short laser pulses with dielectrics. *Journal of Physics B: Atomic, Molecular and Optical Physics*, 41(2):025601, jan 2008. doi: 10.1088/0953-4075/41/2/025601. URL <https://doi.org/10.1088/0953-4075/41/2/025601>.
 58. Baerbel Rethfeld. Free-electron generation in laser-irradiated dielectrics. *Physical Review B*, 73(3):035101, 2006. URL <https://link.aps.org/doi/10.1103/PhysRevB.73.035101>.
 59. Charles Varin, Rhys Emms, Graeme Bart, Thomas Fennel, and Thomas Brabec. Explicit formulation of second and third order optical nonlinearity in the FDTD framework. *Computer Physics Communications*, 222:70–83, 2018. ISSN 0010-4655. doi: <https://doi.org/10.1016/j.cpc.2017.09.018>. URL <https://www.sciencedirect.com/science/article/pii/S0010465517303053>.
 60. R. Courant, K. Friedrichs, and H. Lewy. Über die partiellen Differenzgleichungen der mathematischen Physik. *Mathematische Annalen*, 100:32–74, January 1928. doi: 10.1007/BF01448839.
 61. R. Courant, K. Friedrichs, and H. Lewy. On the partial difference equations of mathematical physics. *IBM Journal of Research and Development*, 11(2):215–234, 1967. doi: <https://doi.org/10.1147/rd.112.0215>.
 62. Vitaly Gruzdev. Modeling of laser-induced ionization of solid dielectrics for ablation simulations: role of effective mass. In Gregory J. Exarhos, Vitaly E. Gruzdev, Joseph A. Menapace, Detlev Ristau, and M. J. Soileau, editors, *Laser-Induced Damage in Optical Materials: 2010*, volume 7842, pages 335 – 345. International Society for Optics and Photonics, SPIE, 2010. doi: 10.1117/12.869760. URL <https://doi.org/10.1117/12.869760>.
 63. Simin Zhang, Michael Tripepi, Abdallah AlShafey, Noah Talisa, Hoang T. Nguyen, Brendan A. Reagan, Emily Sistrunk, David J. Gibson, David A. Alessi, and Enam A. Chowdhury. Femtosecond damage experiments and modeling of broadband mid-infrared dielectric diffraction gratings. *Opt. Express*, 29(24):39983–39999, Nov 2021. doi: 10.1364/OE.439895. URL <https://opg.optica.org/oe/abstract.cfm?URI=oe-29-24-39983>.
 64. T. V. Perevalov, V. A. Gritsenko, S. B. Erenburg, A. M. Badalyan, Hei Wong, and C. W. Kim. Atomic and electronic structure of amorphous and crystalline hafnium oxide: X-ray photoelectron spectroscopy and density functional calculations. *Journal of Applied*

- Physics*, 101(5):053704, 03 2007. ISSN 0021-8979. doi: 10.1063/1.2464184. URL <https://doi.org/10.1063/1.2464184>.
65. W.M. Haynes. *CRC Handbook of Chemistry and Physics, 93rd Edition*. 100 Key Points. Taylor & Francis, 2012. ISBN 9781439880494. URL <https://books.google.com/books?id=-BzP7Rkl7WkC>.
 66. VA Gritsenko, RM Ivanov, and Yu N Morokov. Electronic structure of amorphous SiO₂: Experiment and numerical simulation. *Journal of Experimental and Theoretical Physics*, 81(6):1208–1216, 1995. doi: [https://doi.org/10.1016/S0169-4332\(96\)00944-0](https://doi.org/10.1016/S0169-4332(96)00944-0).
 67. Colin N. Danson, Constantin Haefner, Jake Bromage, Thomas Butcher, Jean-Christophe F. Chanteloup, Enam A. Chowdhury, Almantas Galvanauskas, Leonida A. Gizzi, Joachim Hein, David I. Hillier, and et al. Petawatt and exawatt class lasers worldwide. *High Power Laser Science and Engineering*, 7:e54, 2019. doi: 10.1017/hpl.2019.36.
 68. P. L. Poole, C. Willis, R. L. Daskalova, K. M. George, S. Feister, S. Jiang, J. Snyder, J. Marketon, D. W. Schumacher, K. U. Akli, L. Van Woerkom, R. R. Freeman, and E. A. Chowdhury. Experimental capabilities of 0.4 PW, 1 shot/min scarlet laser facility for high energy density science. *Appl. Opt.*, 55(17):4713–4719, Jun 2016. doi: 10.1364/AO.55.004713. URL <https://opg.optica.org/ao/abstract.cfm?URI=ao-55-17-4713>.
 69. Francis F Chen. *Introduction to Plasma Physics and Controlled Fusion*. Springer International Publishing, 3rd edition, 2016. doi: <https://doi.org/10.1007/978-3-319-22309-4>.
 70. Kevin Werner, Vitaly Gruzdev, Noah Talisa, Kyle Kafka, Drake Austin, Carl M Liebig, and Enam Chowdhury. Single-shot multi-stage damage and ablation of silicon by femtosecond mid-infrared laser pulses. *Scientific reports*, 9(1):1–13, 2019. doi: <https://doi.org/10.1038/s41598-019-56384-0>.
 71. PA Zhokhov and AM Zheltikov. Optical breakdown of solids by few-cycle laser pulses. *Scientific Reports*, 8(1):1–10, 2018. URL <https://doi.org/10.1038/s41598-017-18624-z>.
 72. P. Stampfli and K. H. Bennemann. Theory for the instability of the diamond structure of Si, Ge, and C induced by a dense electron-hole plasma. *Phys. Rev. B*, 42:7163–7173, Oct 1990. doi: 10.1103/PhysRevB.42.7163. URL <https://link.aps.org/doi/10.1103/PhysRevB.42.7163>.
 73. Moritz Grehn, Thomas Seuthe, Michael Höfner, Nils Griga, Christoph Theiss, Alexandre Mermillod-Blondin, Markus Eberstein, Hans Eichler, and Jörn Bonse. Femtosecond-laser induced ablation of silicate glasses and the intrinsic dissociation energy. *Optical Materials Express*, 4(4):689–700, 2014. doi: 10.1364/OME.4.000689.
 74. Hu Wang, Hongji Qi, Jiaoling Zhao, Bin Wang, and Jianda Shao. Transition from isolated sub-micrometer pits to integral ablation of HfO₂ and SiO₂ films under subpicosecond irradiation. *Optics Communications*, 387:214–222, 2017. ISSN 0030-4018. doi: <https://doi.org/10.1016/j.optcom.2016.11.012>. URL <https://www.sciencedirect.com/science/article/pii/S0030401816309774>.
 75. T. Q. Jia, Z. Z. Xu, R. X. Li, D. H. Feng, X. X. Li, C. F. Cheng, H. Y. Sun, N. S. Xu, and H. Z. Wang. Mechanisms in fs-laser ablation in fused silica. *Journal of Applied Physics*, 95(9):5166–5171, 2004. doi: 10.1063/1.1688992. URL <https://doi.org/10.1063/1.1688992>.
 76. Seiji Inaba, Shigeru Fujino, and Kenji Morinaga. Young's modulus and compositional parameters of oxide glasses. *Journal of the American Ceramic Society*, 82(12):3501–3507, 1999. doi: <https://doi.org/10.1111/j.1151-2916.1999.tb02272.x>. URL <https://ceramics.onlinelibrary.wiley.com/doi/abs/10.1111/j.1151-2916.1999.tb02272.x>.
 77. R Paul Drake. Introduction to high-energy-density physics. In *High-Energy-Density Physics*. Springer, 2006. URL https://doi.org/10.1007/3-540-29315-9_1.
 78. Jian Zhao, James Sullivan, John Zayac, and Ted D. Bennett. Structural modification of silica glass by laser scanning. *Journal of Applied Physics*, 95(10):5475–5482, 2004. doi: 10.1063/1.1703832. URL <https://doi.org/10.1063/1.1703832>.
 79. Linjie Zhao, Jian Cheng, Mingjun Chen, Xiaodong Yuan, Wei Liao, Haijun Wang, Qi Liu, and Hao Yang. Toward little heat-affected area of fused silica materials using short pulse and high power CO₂ laser. *Results in Physics*, 12:1363–1371, 2019. ISSN 2211-3797. doi: <https://doi.org/10.1016/j.rinp.2019.01.033>. URL <https://www.sciencedirect.com/science/article/pii/S2211379718330900>.
 80. Dieter Bäuerle. *Laser processing and chemistry*. Springer Science & Business Media, 2013. doi: <https://doi.org/10.1007/978-3-642-17613-5>.
 81. R. G. Kraus, S. T. Stewart, D. C. Swift, C. A. Bolme, R. F. Smith, S. Hamel, B. D. Hammel, D. K. Spaulding, D. G. Hicks, J. H. Eggert, and G. W. Collins. Shock vaporization of silica and the thermodynamics of planetary impact events. *Journal of Geophysical Research: Planets*, 117(E9), 2012. doi: <https://doi.org/10.1029/2012JE004082>. URL <https://agupubs.onlinelibrary.wiley.com/doi/abs/10.1029/2012JE004082>.
 82. RS Khmyrov, SN Grigoriev, AA Okunkova, and AV Gusarov. On the possibility of selective laser melting of quartz glass. *Physics Procedia*, 56:345–356, 2014. doi: <https://doi.org/10.1016/j.phpro.2014>.

- 08.117.
83. Igor S Grigoriev and Evgenii Z Meilikhov. *Handbook of physical quantities*. CRC press, 1997. URL <http://catalog.hathitrust.org/api/volumes/oclc/32468733.html>.
 84. Grigoriĭ Valentinovich Samsonov. *The oxide handbook*. Springer Science & Business Media, 2013. doi: <https://doi.org/10.1007/978-1-4615-9597-7>.
 85. Pauli Virtanen, Ralf Gommers, Travis E. Oliphant, Matt Haberland, Tyler Reddy, David Cournapeau, Evgeni Burovski, Pearu Peterson, Warren Weckesser, Jonathan Bright, Stéfan J. van der Walt, Matthew Brett, Joshua Wilson, K. Jarrod Millman, Nikolay Mayorov, Andrew R. J. Nelson, Eric Jones, Robert Kern, Eric Larson, C J Carey, İlhan Polat, Yu Feng, Eric W. Moore, Jake VanderPlas, Denis Laxalde, Josef Perktold, Robert Cimrman, Ian Henriksen, E. A. Quintero, Charles R. Harris, Anne M. Archibald, Antônio H. Ribeiro, Fabian Pedregosa, Paul van Mulbregt, and SciPy 1.0 Contributors. SciPy 1.0: Fundamental Algorithms for Scientific Computing in Python. *Nature Methods*, 17:261–272, 2020. doi: [10.1038/s41592-019-0686-2](https://doi.org/10.1038/s41592-019-0686-2).
 86. M. Mero, J. Liu, W. Rudolph, D. Ristau, and K. Starke. Scaling laws of femtosecond laser pulse induced breakdown in oxide films. *Phys. Rev. B*, 71:115109, Mar 2005. doi: [10.1103/PhysRevB.71.115109](https://doi.org/10.1103/PhysRevB.71.115109). URL <https://link.aps.org/doi/10.1103/PhysRevB.71.115109>.
 87. Hu Wang, Hongji Qi, Jiaoling Zhao, Bin Wang, and Jianda Shao. Transition from isolated submicrometer pits to integral ablation of HfO₂ and SiO₂ films under subpicosecond irradiation. *Optics Communications*, 387:214–222, 2017. doi: <https://doi.org/10.1016/j.optcom.2016.11.012>.
 88. Chong Wang, Matvei Zinkevich, and Fritz Aldinger. The zirconia–hafnia system: Dta measurements and thermodynamic calculations. *Journal of the American Ceramic Society*, 89(12):3751–3758, 2006. doi: <https://doi.org/10.1111/j.1551-2916.2006.01286.x>. URL <https://ceramics.onlinelibrary.wiley.com/doi/abs/10.1111/j.1551-2916.2006.01286.x>.
 89. W. A. Roth and G. Becker. Ordnungszahl und bildungswärme. *Zeitschrift für Physikalische Chemie*, 159A(1):1–26, 1932. doi: [doi:10.1515/zpch-1932-15902](https://doi.org/10.1515/zpch-1932-15902). URL <https://doi.org/10.1515/zpch-1932-15902>.
 90. G. L. Humphrey. Heats of formation of hafnium oxide and hafnium nitride. *Journal of the American Chemical Society*, 75(12):2806–2807, 1953. doi: [10.1021/ja01108a004](https://doi.org/10.1021/ja01108a004). URL <https://doi.org/10.1021/ja01108a004>.
 91. Elmer J. Huber and Charles E. Holley. Enthalpy of formation of hafnium dioxide. *Journal of Chemical & Engineering Data*, 13(2):252–253, 1968. ISSN 0021-9568. doi: [10.1021/jc60037a034](https://doi.org/10.1021/jc60037a034). URL <https://doi.org/10.1021/jc60037a034>.
 92. A.N. Kornilov, I.M. Ushakova, E.J. Huber, and C.E. Holley. The enthalpy of formation of hafnium dioxide. *The Journal of Chemical Thermodynamics*, 7(1):21–26, 1975. ISSN 0021-9614. doi: [https://doi.org/10.1016/0021-9614\(75\)90076-2](https://doi.org/10.1016/0021-9614(75)90076-2). URL <https://www.sciencedirect.com/science/article/pii/0021961475900762>.
 93. YN Paputskii, VA Krzhizhanovskaya, and VB Glushkova. Enthalpy of formation of rare earth hafnates and zirconates. *Inorg. Mater*, 10(8): 1338–9, 1974.
 94. M. B. Panish and Liane Reif. Thermodynamics of the vaporization of Hf and HfO₂: Dissociation energy of HfO. *The Journal of Chemical Physics*, 38(1):253–256, 1963. doi: [10.1063/1.1733473](https://doi.org/10.1063/1.1733473). URL <https://doi.org/10.1063/1.1733473>.
 95. John J. Low, Noah H. Paulson, Michael D’Mello, and Marius Stan. Thermodynamics of monoclinic and tetragonal hafnium dioxide (HfO₂) at ambient pressure. *Calphad*, 72, 11 2020. ISSN 0364-5916. doi: [10.1016/j.calphad.2020.102210](https://doi.org/10.1016/j.calphad.2020.102210). URL <https://www.osti.gov/biblio/1762259>.
 96. Ghita Geoffroy, Guillaume Duchateau, Nikita Fedorov, Patrick Martin, and Stéphane Guizard. Influence of electron coulomb explosion on photoelectron spectra of dielectrics irradiated by femtosecond laser pulses. *Laser Physics*, 24(8):086101, 7 2014. doi: [10.1088/1054-660X/24/8/086101](https://doi.org/10.1088/1054-660X/24/8/086101). URL <https://dx.doi.org/10.1088/1054-660X/24/8/086101>.
 97. G G Paulus, W Becker, W Nicklich, and H Walther. Rescattering effects in above-threshold ionization: a classical model. *Journal of Physics B: Atomic, Molecular and Optical Physics*, 27(21):L703, nov 1994. doi: [10.1088/0953-4075/27/21/003](https://doi.org/10.1088/0953-4075/27/21/003). URL <https://dx.doi.org/10.1088/0953-4075/27/21/003>.
 98. Guillaume Duchateau, Ghita Geoffroy, Anthony Dyan, Hervé Piombini, and Stéphane Guizard. Electron-hole dynamics in normal and deuterated kh₂po₄ illuminated by intense femtosecond laser pulses. *Phys. Rev. B*, 83:075114, Feb 2011. doi: [10.1103/PhysRevB.83.075114](https://doi.org/10.1103/PhysRevB.83.075114). URL <https://link.aps.org/doi/10.1103/PhysRevB.83.075114>.
 99. Drake R. Austin, Kyle R. P. Kafka, Yu Hang Lai, Zhou Wang, Cosmin I. Blaga, and Enam A. Chowdhury. Femtosecond laser damage of germanium from near- to mid-infrared wavelengths. *Opt. Lett.*, 43(15):3702–3705, Aug 2018. doi: [10.1364/OL.43.003702](https://doi.org/10.1364/OL.43.003702). URL <https://opg.optica.org/ol/abstract.cfm?URI=ol-43-15-3702>.
 100. Joseph R Smith, Chris Orban, John T Morrison, Kevin M George, Gregory K Ngirmang, Enam A Chowdhury, and W Mel Roquemore. Optimizing

- laser–plasma interactions for ion acceleration using particle-in-cell simulations and evolutionary algorithms. *New Journal of Physics*, 22(10):103067, 2020. doi: 10.1088/1367-2630/abbfce.
101. John Burkardt. Fortran90 codes. https://people.sc.fsu.edu/~jburkardt/f_src/f_src.html. Accessed: 2025-04-22.
 102. WJ Cody, Kathleen A Paciorek, and Henry C Thacher. Chebyshev approximations for dawson’s integral. *Mathematics of Computation*, 24(109):171–178, 1970.
 103. Ohio Supercomputer Center. Ohio supercomputer center, 1987. URL <http://osc.edu/ark:/19495/f5s1ph73>.
 104. J. D. Hunter. Matplotlib: A 2D graphics environment. *Computing in Science & Engineering*, 9(3):90–95, 2007. doi: 10.1109/MCSE.2007.55.
 105. Charles R. Harris, K. Jarrod Millman, Stéfan J. van der Walt, Ralf Gommers, Pauli Virtanen, David Cournapeau, Eric Wieser, Julian Taylor, Sebastian Berg, Nathaniel J. Smith, Robert Kern, Matti Pícus, Stephan Hoyer, Marten H. van Kerkwijk, Matthew Brett, Allan Haldane, Jaime Fernández del Río, Mark Wiebe, Pearu Peterson, Pierre Gérard-Marchant, Kevin Sheppard, Tyler Reddy, Warren Weckesser, Hameer Abbasi, Christoph Gohlke, and Travis E. Oliphant. Array programming with NumPy. *Nature*, 585(7825):357–362, September 2020. doi: 10.1038/s41586-020-2649-2. URL <https://doi.org/10.1038/s41586-020-2649-2>.